MOLECULAR
METABOLISM

Intestinal SEC16B modulates obesity by regulating chylomicron metabolism

Ruicheng Shi [1], Wei Lu [1], Ye Tian [1], Bo Wang [1,2,3,*]

ABSTRACT

Objective: Genome-wide association studies (GWAS) have identified genetic variants in SEC16 homolog B (*SEC16B*) locus to be associated with obesity and body mass index (BMI) in various populations. *SEC16B* encodes a scaffold protein located at endoplasmic reticulum (ER) exit sites that is implicated to participate in the trafficking of COPII vesicles in mammalian cells. However, the function of SEC16B *in vivo*, especially in lipid metabolism, has not been investigated.

Methods: We generated *Sec16b* intestinal knockout (IKO) mice and assessed the impact of its deficiency on high-fat diet (HFD) induced obesity and lipid absorption in both male and female mice. We examined lipid absorption in *vivo* by acute oil challenge and fasting/HFD refeeding. Biochemical analyses and imaging studies were performed to understand the underlying mechanisms.

Results: Our results showed that *Sec16b* intestinal knockout (IKO) mice, especially female mice, were protected from HFD-induced obesity. Loss of *Sec16b* in intestine dramatically reduced postprandial serum triglyceride output upon intragastric lipid load or during overnight fasting and HFD refeeding. Further studies showed that intestinal *Sec16b* deficiency impaired apoB lipidation and chylomicron secretion.

Conclusions: Our studies demonstrated that intestinal SEC16B is required for dietary lipid absorption in mice. These results revealed that SEC16B plays important roles in chylomicron metabolism, which may shed light on the association between variants in *SEC16B* and obesity in human.

1. INTRODUCTION

The prevalence of obesity and its associated metabolic disorders is rising dramatically due to sedentary lifestyle and increased fat consumption [1,2]. The intestine plays a central role in lipid absorption, in which lipids are incorporated into triglyceride-rich chylomicrons and transported into circulation [3,4]. It has been shown that elevated chylomicron production contributes to the dyslipidemia in metabolic disorders, such as obesity, diabetes and cardiovascular diseases [5]. However, the biogenesis and transportation of chylomicron have not been fully understood. In enterocytes, dietary lipids are transferred to apolipoprotein B48 (apoB48) by microsomal triglyceride transfer protein (MTTP) in the endoplasmic reticulum (ER) to form prechylomicrons [6], which are subsequently transported to the Golgi apparatus via prechylomicron transport vesicles (PCTVs) [7]. The trafficking of PCTVs from the ER to the Golgi involves a cascade of complex processes, including their exit from the ER and delivery to the Golgi [8]. Their exit from the ER is considered to be the rate-limiting step in chylomicron secretion from enterocyte [9,10]. Biochemical analysis identified several protein components in PCTVs, such as cluster of differentiation 36 (CD36), liver-type fatty acid binding protein (L-FABP), and subunits of coat protein II (COPII) machinery [7,11—14]. The function of these proteins in PCTV formation and transportation has not been fully

elucidated. Upon fusion to the Golgi, prechylomicrons are further lipidated and secreted into lymphatics as mature chylomicrons.

Genome-wide association studies (GWAS) have identified several single-nucleotide polymorphisms (SNPs) in various genes to be associated with obesity and body mass index (BMI). One of these genes, *SEC16B*, has been linked to obesity in different populations [15—23]. SEC16B is the shorter mammalian orthologue of *S. cerevisiae* SEC16, which was first identified as a scaffold protein that organizes ER exit sites (ERES) by interacting with COPII components [24,25]. *SEC16B* encodes a 117 kD protein that was previously described as a regucalcin gene promoter region-related protein (RGPR-p117) [26]. However, the role of SEC16B as a transcription factor has not been confirmed because there is no evidence that SEC16B directly binds to regucalcin gene promoter region [27,28]. A previous study demonstrated that SEC16B regulates the transport of peroxisomal membrane biogenesis factor, PEX16, from the ER to peroxisomes in mammalian cells, and thus may participate in the formation of new peroxisomes derived from the ER [29]. However, the significance of this regulation is unclear. Nevertheless, the pathophysiological functions of SEC16B *in vivo* and whether SEC16B may contribute to the pathogenesis of obesity have not been investigated.

In this study, we examined the role of SEC16B in lipid metabolism in the intestine using *Sec16b* intestinal specific knockout (IKO) mice. Our

[1]Department of Comparative Biosciences, College of Veterinary Medicine, University of Illinois at Urbana-Champaign, Urbana, IL, USA [2]Division of Nutritional Sciences, College of Agricultural, Consumer and Environmental Sciences, University of Illinois at Urbana-Champaign, Urbana, IL, USA [3]Cancer Center at Illinois, University of Illinois at Urbana-Champaign, Urbana, IL, USA

*Corresponding author. 3840 VMBSB, 2001 S Lincoln Ave, Urbana, IL 61802, USA. E-mail: bowang@illinois.edu (B. Wang).

data demonstrate that SEC16B plays important roles in chylomicron production in the intestine. *Sec16b* deficiency leads to marked reduction in triglyceride output in serum in the context of bolus lipid challenge. We show that loss of *Sec16b* impairs chylomicron lipidation and secretion from enterocytes. Consequently, *Sec16b* IKO mice are protected from high-fat diet (HFD) induced obesity and glucose intolerance. These data identify SEC16B as a novel regulator of chylomicron production and may provide insight into the association between genetic variants in *SEC16B* and obesity in human.

2. MATERIALS AND METHODS

2.1. Animal models
We generated *Sec16b* intestinal specific knockout mice (IKO) from *Sec16b*[tm1a(KOMP)Wtsi] (MMRRC_049583_UCD) mice, in which the targeted allele is "conditional-ready". We first crossed heterozygous *Sec16b*[tm1a(KOMP)Wtsi] mice with mice expressing a *Flpe* recombinase deleter transgene (B6.Cg-Tg(ACTFLPe)9205Dym/J) to remove the gene-trapping cassette in intron 12 of *Sec16b*, producing a conditional knockout allele (*Sec16b*[F/+]) containing loxP sites in intron 12 and intron 13. *Sec16b*[F/F] mice were crossed with *villin-Cre* transgenic mice (B6.Cg-Tg(Vil1-cre)997Gum/J) to generate *Sec16b*[F/F], *Villin-Cre +* (IKO) mice. *Sec16b*[F/F], *Villin-Cre −* mice were used as controls.

2.2. Mouse studies
All animal procedures were conducted in compliance with protocol (#21200) approved by the Institutional Animal Care and Use Committee (IACUC) at University of Illinois at Urbana−Champaign (UIUC). All mice were housed under pathogen-free conditions in a temperature-controlled room with a 12 h light/dark cycle. All mice were subjected to either chow diet or HFD (60% calories from fat, Research Diets #D12492). All mice were fasted for 6 h prior experiments unless stated otherwise. Small intestine samples were flushed with cold PBS and collected at different regions (duodenum, jejunum and ileum) corresponding to a length ratio of 1:2:1. All samples were snap frozen in liquid nitrogen and stored in −80 °C, or fixed in 10% formalin, or frozen in OCT for cryosectioning. Blood was collected by retro-orbital bleeding, and the plasma was separated by centrifugation. Plasma lipids were measured with Wako triglyceride kit, Wako Free Cholesterol E kit, the Wako Cholesterol E kit, the Wako HR series NEFA-HR (2) kit (FUJIFILM, Richmond, VA), and the Infinity Triglyceride Reagent kit (Thermo Fisher, Waltham, MA). Tissue and fecal lipids were extracted with Folch lipid extraction [30] and measured with the same enzymatic kits. For glucose tolerance tests (GTT), mice were fasted for 6 h and i.p. injected with D-Glucose (1 g/kg body weight), blood glucose levels were measured at 0, 15, 30, 60 and 90 min. The plasma lipoprotein lipase (LPL) activities were measured with a lipoprotein lipase assay kit (Abcam, Cambridge, United Kingdom). Tissue histology was performed in the UIUC Comparative Biosciences Histology Laboratory.

2.3. Postprandial lipid absorption assay
For lipid absorption assay, mice were fasted for 4 h and gavaged with corn oil (10 µg/g body weight). Plasma was collected through tail vein at 0, 1, 2, 4 and 6 h and plasma lipids were measured with Wako HR series NEFA-HR (2) kit and Wako triglyceride kit. For lipid absorption assay with lipoprotein lipase inhibitor, mice were fasted, gavaged with corn oil and retro-orbitally injected with Tyloxapol (500 mg/kg body weight). Plasma was collected at 0, 1, 2, 3 and 4 h. Plasma fast protein liquid chromatography (FPLC) lipoprotein profiles were performed at Lipid Core of Vanderbilt University School of Medicine.

2.4. *Ex vivo* fatty acid uptake assay
The detailed procedures have been described previously [31]. In brief, mice were sacrificed and small intestines were immediately removed and rinsed with PBS. A segment of the proximal duodenum was clamped with hemostats forceps and incubated with QBT FA uptake-assay solution (Molecular Devices, San Jose, CA) mixed with 10 mM sodium taurocholate (Sigma-Aldrich, St. Louis, MO) and 4 mM oleic acid for either 1 or 2 min. Villi were then obtained from the sac and were washed twice with ice cold 0.5 mM sodium taurocholate and homogenized with RIPA buffer. Fluorescence signals were then measured from the supernatant and normalized to the protein concentrations.

2.5. Imaging studies
Mice were fasted for 4 h and gavaged with BODIPY™ 500/510 C1, C12 (2 µg/g body weight) in corn oil (10 µl/g body weight). After 2 h, small intestines (duodenum and jejunum) were harvested and embedded in OCT. Samples were sectioned into 10 µm sections, immediately mounted in ProLong™ Diamond Antifade Mountant with DAPI and examined under fluorescence microscope. For fasting and HFD refeeding experiment, mice were fasted overnight and refed with HFD for 2 h either with or without Tyloxapol injection. Duodenum and jejunum were harvested, embedded, and sectioned as described above. Slides were then fixed in 4% paraformaldehyde for 5 min, stained in Oil-Red-O for 10 min and counterstained with hematoxylin. For determination of chylomicron size by transmission electron microscopy (TEM), 100 µl pooled plasma from 4 *Sec16b* IKO and *Sec16b*[F/F] control mice were overlaid with 700 µl saline and centrifuged at 55, 000 rpm for 5 h in a TLA 100.3 rotor and the top layer was collected. For electron microscopy analysis, 5 µl of the chylomicron fraction was applied to carbon-coated copper grids and stained with 2.0% uranyl acetate for 15 min. Grids were visualized with a JEOL 100CX transmission electron microscope. Particle diameter was measured using ImageJ.

2.6. Immunohistochemistry analysis
For F4/80 staining, the paraffin sections were rehydrated and subjected to antigen retrieval for 20 min in near boiling citric buffer (pH 6.0). Slides were blocked with goat serum for 1 h at room temperature and incubated with F4/80 antibodies (BM8, BioLegend, San Diego, CA) overnight at 4 °C. Slides were then washed and incubated with Biotin-conjugated secondary antibodies (Vector Laboratories, Newark, CA) and signals were developed with a ABC kit (Vector Laboratories, Newark, CA).

2.7. Transmission electron microscopy analysis of intestine
Transmission electron microscopy analysis of intestine samples was performed at Materials Research Laboratory at UIUC and Electron Microscopy Core of University of Illinois at Chicago. Briefly, control and IKO mice were fasted overnight and refed HFD for 2 h before sacrificing. Upon refeeding, mouse tissues (duodenum and jejunum) were collected and fixed immediately in Sorenson's Phosphate Buffer mixture containing 2% paraformaldehyde and 2.5% glutaraldehyde. The samples were then rinsed in phosphate buffer, incubated in Osmium tetroxide with potassium ferrocyanide, and rinsed with water. Samples were en-bloc stained with filtered uranyl acetate overnight and dehydrated in ethanol series. Samples were then subsequently infiltrated with 1:1 and 1:4 acetonitrile: epoxy mixture and finally infiltrated with Lx112 epoxy mixture (Ladd, Inc), and hardened at 80 °C for 2 days. After embedding, samples were trimmed, and cut into 90−100 nm sections with a diamond knife. Sections were stained with

Uranyl Acetate and Lead Citrate and were visualized on a Hitachi H600 Electron Microscope at 75 KV. Images were taken with plate film and scanned at 3200 dpi for digital images.

2.8. Endoplasmic reticulum and Golgi fractionation from enterocyte

The ER and Golgi fractions were isolated from enterocytes as described [7]. In brief, enterocytes were harvested from overnight fasting and HFD refed control and IKO mice following previous publication [31]. 2×10^7 cells were lysed in buffer A (0.25 M Sucrose, 5 mM EDTA, 10 mM HEPES, protease inhibitor cocktail) and homogenized using a motor driven homogenizer (Caframo, Ontario, Canada). The homogenate was spun at 8,500 g for 10 min at 4 °C, and the resulting supernatant was further spun at 100,000g for 3 h at 4 °C. The pellets were collected, density adjusted with 1.22 ml 1.22M sucrose solution, the resuspended mixture was then overlaid with 1 ml 1.15 M, 1 ml 0.86 M and 0.7 ml 0.25 M sucrose solution. This discontinuous gradient was spun at 82,000g for 3 h at 4 °C. Golgi fraction was enriched at 0.25/0.86 and 0.86/1.15 interface, while ER/microsomal membrane remained in the 1.22 M sucrose layer and/or appeared as a pellet. All fractions were collected with the same volume.

2.9. Crypt isolation and enteroid monolayer culture

Briefly, mice were sacrificed, and duodenums and jejunums were immediately removed, flushed with cold PBS and cut open longitudinally. The tissues were washed twice with cold PBS and gently rocked at 4 °C with PBS containing 2.5 mM EDTA for 30 min. Intestines were then vortexed vigorously for 30 s in 3 s pulses to release crypts. The intestine was then sat on ice for 10min to allow villi to settle down. Supernatant containing crypts were obtained, passed through 70 μm filter, and centrifuged at $100 \times g$ for 3 min to pellet the crypts. The collected pellet was then washed once with PBS and resuspended in attachment media (IntestiCult Organoid Growth Medium (OGM) (STEMCELL technologies, Vancouver, BC) supplemented with LDN-193189 (1 μM, Sigma-Aldrich, St. Louis, MO) and CHIR99021 (3 μM, Selleck Chemicals, Huston, TX)). Before seeding, 24-well plates were first coated with OGM mixed with growth factor reduced Matrigel (Corning, New York, NY) at a ratio of 30:1 at 37 °C for 1 h. During seeding, ∼5000 crypts were seeded into each well and incubated in attachment media for 4 h to allow for proper attachment. The non-adherent fragments were then aspirated and attached crypts were incubated in OGM for the remainder of the culture. After overnight incubation, enteroid monolayers were treated with 400 μM oleic acid (Sigma-Aldrich, St. Louis, MO) for 6 h and cells were harvested for either RNA or protein extraction.

2.10. Quantitative PCR

In brief, tissue was homogenized with TissueLyser II (Qiagen, Hilden, Germany), and total RNA was extracted with TRIzol (Invitrogen, Waltham, MA). cDNA was synthesized, and gene expression was quantified by CFX384 Touch Real-Time PCR Detection System (Bio-Rad, Hercules, CA) with SYBR Green (Bio-Rad, Hercules, CA). Gene expression levels were normalized to 36B4.

2.11. Western blot analysis

Intestine tissue was homogenized by TissueLyser II in RIPA buffer (50 mM Tris—HCl, pH 7.4, 150 mM NaCl, 1% NP-40, 0.5% sodium deoxycholate, 0.1% SDS) supplemented with protease and phosphatase inhibitors and PMSF. Lysates were sonicated and supernatant was collected by centrifugation. Protein lysates, sera, or chylomicron fractions were mixed with $4\times$ laemmli buffer and loaded onto 4%—15% TGX Gels (Bio-Rad, Hercules, CA), transferred to hybond PVDF

membrane (GE Healthcare, Chicago, IL), and incubated with the following antibodies: anti-APOB (ab20737, Abcam), anti-MTTP (sc-135994, Santa Cruz Biotechnology), GAPDH (MAB374, EMD Millipore). After incubation with secondary antibodies, the protein bands were visualized with enhanced chemiluminescence (ECL) (Thermo Fisher, Waltham, MA).

2.12. Indirect calorimetry and body composition measurements

Metabolic rates were measured by indirect calorimetry in open-circuit Oxymax chambers in the Comprehensive Lab Animal Monitoring System (CLAMS) (Columbus Instruments). Mice fed with HFD for 10—12 weeks were placed individually in metabolic chambers of the CLAMS (Columbus Instruments, Columbus, OH) for one week. The chamber was maintained at 23 °C with 12 h light/dark cycles. Food and water were provided as needed. Oxygen consumption rate (VO_2), carbon dioxide production (VCO_2) rates, food intake, respiratory exchange ratio (RER) and physical activities (x-tot) were measured every 12 min over a period of 4 days. The first readings were taken after a 36 h acclimation period and data were presented as a 3 day average line chart. Body compositions (whole-body fat and lean composition) were measured on Echo MRI (Echo Medical Systems, Houston, TX).

2.13. Statistical analysis

Sample sizes were determined based on our previous studies and preliminary results. All results were confirmed in at least two different batches of mice. Results from quantitative experiments were expressed as means ± SEM. GraphPad Prism 9.0 (San Diego, CA) was used for all statistical analyses. Where appropriate, significance was calculated by Student's t test, one- or two-way ANOVA with Tukey's or Sidak's multiple comparison test.

3. RESULTS

3.1. Sec16b IKO mice do not show noticeable phenotype on chow diet

We first examined the expression of Sec16b in different segments of mouse intestine. As shown in Fig. S1A, Sec16b is highly expressed in the small intestine compared to colon (Fig. S1A). To examine the function of SEC16B in the intestine, we generated Sec16b intestinal specific knockout mice (IKO) from $Sec16b^{tm1a(KOMP)Wtsi}$ mice, in which the targeted allele is "conditional-ready". We crossed heterozygous $Sec16b^{tm1a(KOMP)Wtsi}$ mice with mice expressing a Flpe transgene to produce a floxed allele. Floxed mice ($Sec16b^{F/F}$) were further bred with Villin-Cre transgenic mice to delete Sec16b exon 13 in the intestine (Figure 1A). Real-time RT-PCR analysis revealed a ∼97% reduction in Sec16b mRNA levels in both male and female IKO mice compared to floxed Cre-negative (F/F) control mice (Figure 1B). No difference in body weight was observed in either male or female IKO mice compared to their F/F littermates on chow diet (Figure 1C). Serum triglyceride (TG) and total or free cholesterol levels were comparable between IKO and control in both male and female mice (Figs. S1B—S1D). Interestingly, male IKO mice showed a small but significant decrease in serum non-esterified fatty acid (NEFA) levels compared to control mice (Fig. S1E). In contrast, female IKO mice displayed a slight increase in serum NEFA levels (Fig. S1E). There was no discernible difference in the histology of intestine of IKO mice compared to controls (Figure 1D).

3.2. Sec16b IKO mice are protected from HFD-induced obesity

To further explore if SEC16B may be involved in the pathogenesis of obesity, we challenged IKO and control mice with HFD starting at 8 weeks of age. Both male and female IKO mice showed significantly
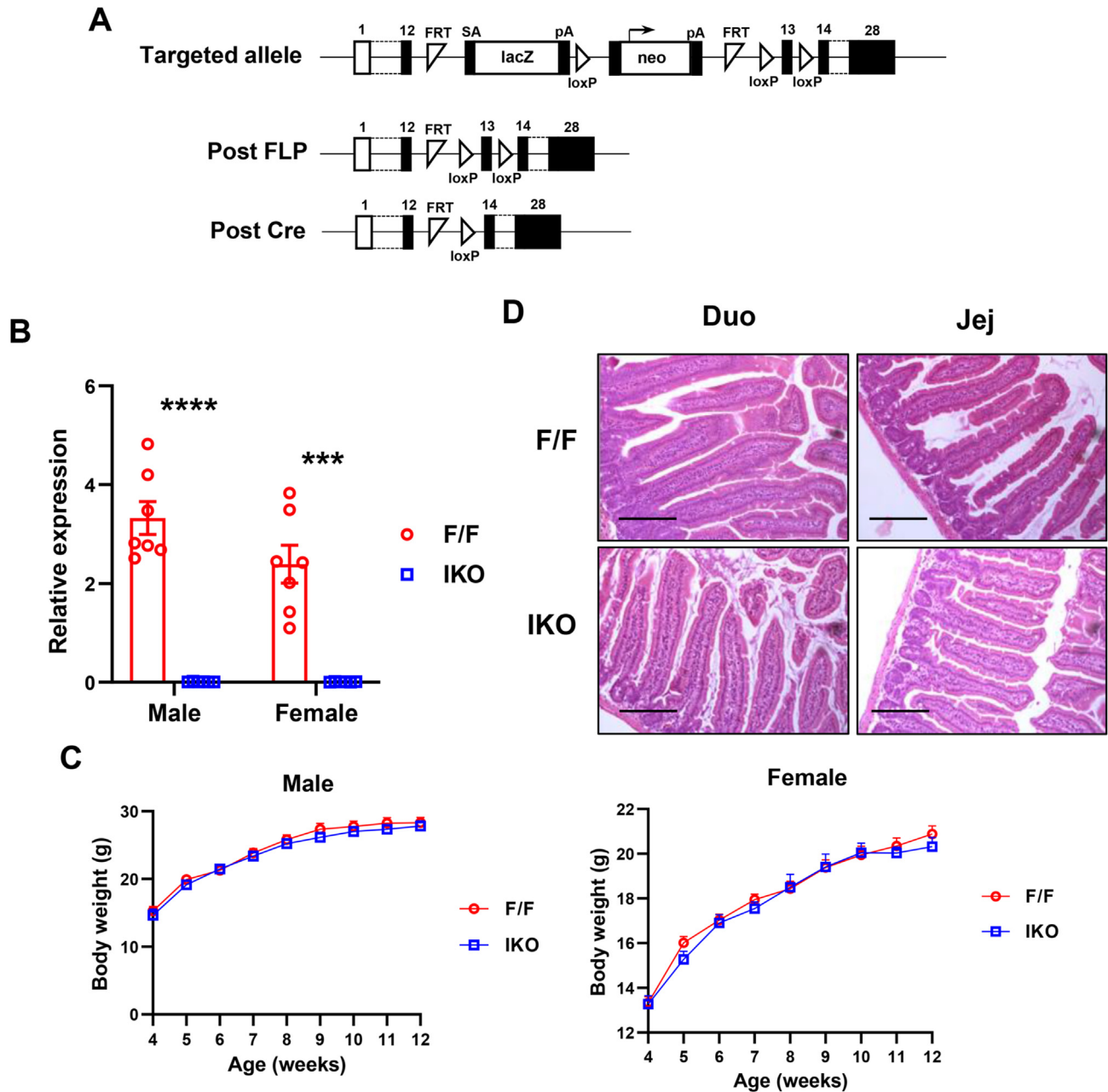
Figure 1: *Sec16b* IKO mice are normal on chow diet. **(A)** Strategy for generating intestine specific *Sec16b* knockout mice. *Sec16b*$^{-/+}$ mice carrying the conditional-ready knockout allele were mated with Flpe transgenic mice to generate the *Sec*16b$^{F/F}$ mice. *Sec*16b$^{F/F}$ mice were bred with *Villin*-Cre transgenic mice to generate intestine specific *Sec16b* knockout mice. **(B)** Expression of *Sec16b* in the intestine of *Sec*16b$^{F/F}$ (F/F) and *Sec*16b$^{F/F}$ *Villin*-Cre (IKO) mice (n = 6−7/group). **(C)** Growth curve of control (F/F) and IKO mice on chow diet (n = 6−8/group). **(D)** Representative histology of duodenum and jejunum from chow diet fed control and IKO mice. Scale bar: 100 μm. Values are means ± SEM. Statistical analysis was performed with Student's t test. **P < 0.01.

less body weight gain compared to control littermates after 12−14 weeks of HFD feeding (Figure 2A,B). Interestingly, female mice showed more pronounced body weight difference between IKO and controls than that in male mice. Magnetic Resonance Imaging (MRI) analysis of body composition showed that the body weight difference after HFD feeding was primarily due to reduced body fat in female mice, especially subcutaneous white adipose tissue (scWAT) (Figure 2C, Figure S2). The total body fat mass in male IKO also trended to be less compared to control mice, despite no significant difference in epidydimal or subcutaneous WAT (Figure 2C, Figure S2). In contrast, lean mass was not changed in both female and male mice (Figure 2D). Both male and female IKO mice showed improved glucose clearance in glucose tolerance test (Figure 2E,F), likely due to less HFD-induced obesity in IKO mice since no difference was observed in chow diet fed mice (Figs. S3A—S3B). Serum lipid analysis revealed no difference in TG, NEFA, free cholesterol or cholesterol levels between IKO and control mice after 6 h fasting (Figs. S4A—S4D).

Histology analysis of HFD-fed mice revealed more lipid accumulation in IKO intestines compared to controls (Figure 2G), indicating that chylomicron output may be impaired in the absence of SEC16B. Consistently,
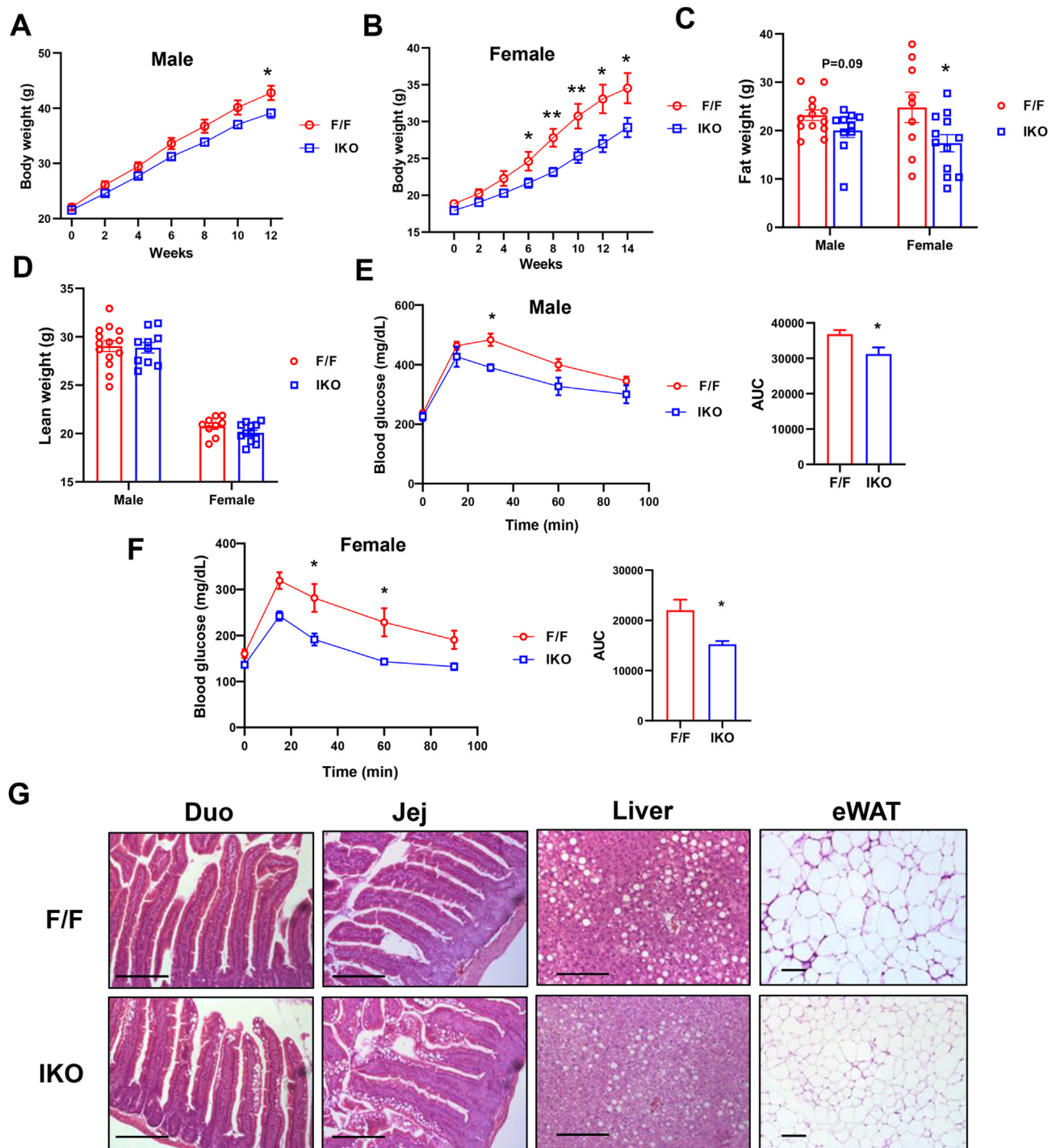
Figure 2: *Sec16b* IKO mice are protected from HFD-induced obesity. (A and B) Growth curve of male (A) and female (B) control (F/F) and IKO mice on HFD (n = 9−14/group). **(C and D)** Fat (C) and lean (D) mass in HFD-fed control (F/F) and IKO mice (n = 9−14/group). **(E and F)** GTT analysis of male (E) and female (F) control (F/F) and IKO mice on HFD (n = 4−8/group). **(G)** Representative histology of HFD-fed control (F/F) and IKO mice. Values are means ± SEM. Statistical analysis was performed with Student's t test (A-D), and two-way ANOVA (E-F). *P < 0.05, **P < 0.01.

IKO mice showed much smaller adipocytes and less infiltration of inflammatory cells in epididymal WAT compared to control mice (Figure 2G and Figs. S4E—S4F), which may contribute to the improved glucose tolerance in IKO mice. Hepatic TG, NEFA and total cholesterol levels were comparable between IKO and control mice (Figs. S4G—S4J), while free cholesterol levels were slightly lower in male IKO mice.

Next, we sought to understand the cause of reduced body weight gain in IKO mice fed HFD. The expression of most of the genes involved in fatty acid (FA) uptake, TG synthesis, lipoprotein production and intracellular transport was not altered in IKO intestines compared to controls (Figs. S5A and S5B). Thus, the expression in lipid metabolic genes could not explain the phenotypes of IKO mice.

Next, we measured daily food consumption in individually housed HFD fed mice. Both male and female *Sec16b* IKO mice consumed a similar amount of food as controls (Figure 3A), suggesting that the resistance to HFD-induced body weight gain was not due to reduced food consumption in IKO mice. There was no difference in fecal TG and NEFA levels between IKO and control mice (Figure 3B,C), indicating that loss of *Sec16b* does not affect lipid uptake from intestinal lumen into enterocytes. Then we measured energy metabolism in mice fed HFD for 8 weeks by indirect calorimetry using the Comprehensive Lab Animal Monitoring System (CLAMS). As shown in Figure 3D,E, oxygen consumption, CO_2 production, and energy expenditure (EE) were increased and trended towards an increase in female and male IKO mice, respectively. Respiratory exchange ratio (RER) was not altered in both female and male IKO mice, while cumulative physical activity was increased in female, but to a lesser extent in male IKO mice (Figs. S6A

and S6B). Thus, the more pronounced increase in EE and physical activity in female IKO mice compared to male IKO mice likely contributes to the sex difference in body weight gain in HFD-fed IKO mice.

3.3. *Sec16b* deficiency in the intestine impairs chylomicron output

Given more lipid accumulation in IKO enterocytes, we postulated that SEC16B may be involved in transport of dietary fat into the circulation. To test this, we performed postprandial TG response assays. We gavaged IKO and control mice with a bolus of corn oil and monitored serum TG and NEFA levels at different time points. As expected, serum TG and NEFA levels gradually increased and peaked at 2 h post gavaging in control mice (Figure 4A,B). In contrast, serum TG and NEFA levels remained very low in IKO mice during the entire course. Insulin is known to activate lipoprotein lipase (LPL) and increase the hydrolysis of lipoproteins and serum NEFA levels. However, insulin levels were
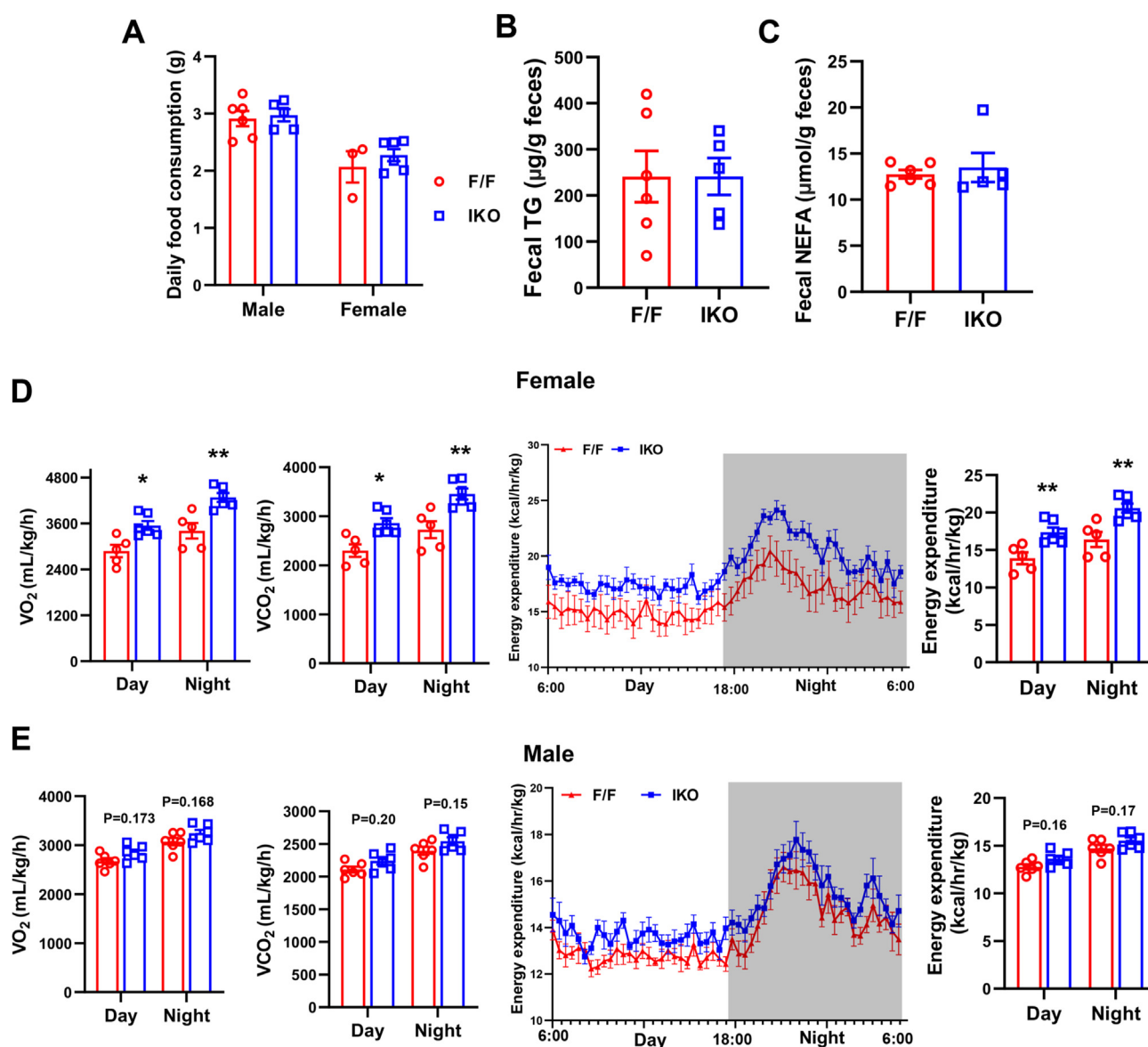
Figure 3: Loss of *Sec16b* increases energy expenditure. (A) Daily food consumption of control (F/F) and IKO mice on HFD (n = 5−6/group). **(B and C)** Fecal TG and NEFA levels of control (F/F) and IKO mice on HFD (n = 5−6/group). **(D and E)** CLAMS analysis of oxygen consumption rate, CO_2 production rate, and energy expenditure (EE) of control (F/F) and IKO mice on HFD (n = 5−6/group). Values are means ± SEM. Statistical analysis was performed with Student's t test (A-C) and two-way ANOVA (D and E).
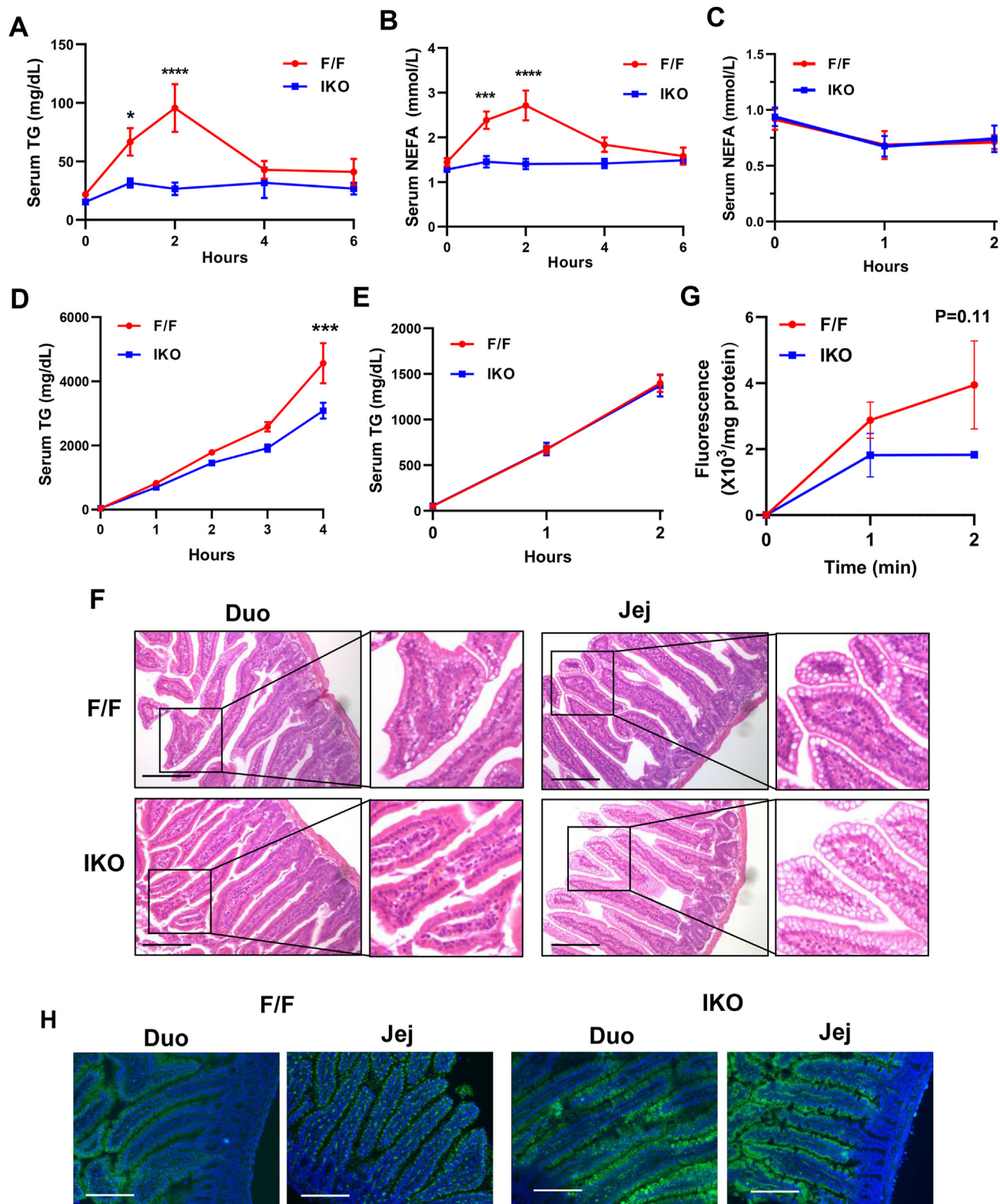
Figure 4: *Sec16b* deficiency in the intestine impairs lipid absorption when challenged with corn oil bolus. **(A and B)** Postprandial TG and NEFA response in control (F/F) and IKO mice after oral gavage with corn oil (10 μl/g BW) (n = 9–11/group). **(C–D)** Postprandial NEFA and TG response in control (F/F) and IKO mice injected with Tyloxapol followed by oral gavage with corn oil (10 μl/g BW) (n = 6/group). **(E)** VLDL-TG secretion in control (F/F) and IKO mice. Mice were fasted for 4 h followed by retro-orbital injection of Tyloxapol (n = 6/group). **(F)** Representative histology of intestine sections from control (F/F) and IKO mice after oral gavage with corn oil for 2 h. Scale bar: 100 μm. **(G)** *Ex vivo* FA uptake in duodenum of male control (F/F) and IKO mice. Mice were fasted 4 h followed by FA uptake assay as described in the methods (n = 3/group).**(H)** Fluorescence images of small intestines of control (F/F) and IKO mice after oral gavage with olive oil containing BODIPY-labeled fatty acid for 2 h. Scale bar: 100 μm. Values are means ± SEM. Statistical analysis was performed with two-way ANOVA (A-E, G). *$P < 0.05$, ***$P < 0.001$, ****$P < 0.0001$.

comparable between control and IKO mice upon oil gavage (Figs. S7A—S7B). Moreover, there was no difference in serum LPL activity between control and IKO mice (Figs. S7C—S7E), suggesting that the difference in serum TG and NEFA levels was not caused by insulin action or altered LPL activity. We reasoned that the profound reduction in serum NEFA levels in IKO mice is likely caused by less chylomicron available for lipase hydrolysis. Indeed, administration of lipase inhibitor, Tyloxapol, reduced NEFA levels in control mice to similar levels in IKO mice during lipid tolerance test (Figure 4C), suggesting that increased serum NEFA levels are mainly derived from chylomicron TG hydrolysis during oral lipid challenge. Surprisingly, the difference in serum TG levels between control and IKO mice was dampened upon Tyloxapol treatment (Figure 4D). We reasoned that continuous VLDL secretion may obscure the difference in serum TG after lipase inhibition. Indeed, serum TG levels in Tyloxapol treated fasted mice were drastically increased to comparable levels in both genotypes (Figure 4E). Western blot analysis revealed dramatic increase in both apoB100 and apoB48 protein levels upon Tyloxapol injection and oil gavage (Fig. S8). Moreover, apoB48 levels were reduced in IKO mice after 2 h post treatment, corroborating impaired lipid output in the absence of SEC16B.

Histology analysis showed marked lipid accumulation in IKO intestines following oil gavage compared to control intestines (Figure 4F), indicating that loss of SEC16B impairs lipid secretion from enterocytes into circulation. FA uptake into enterocytes is the first step in lipid absorption. Quantification of FA uptake showed that loss of *Sec16b* reduced FA uptake in IKO mice (P = 0.11) (Figure 4G). However, when we gavaged mice with BODIPY-labeled FA together with corn oil, abundant fluorescence-labeled lipid droplets were observed in IKO intestines, while very little fluorescence was present in controls (Figure 4H), suggesting that the reduced FA uptake by *Sec16b* deficiency was unlikely a major contributor to the defective TG output.

To further determine if intestinal SEC16B regulates lipid absorption, we fasted chow diet fed control and IKO mice overnight and refed them with HFD for 2 h. As shown in Figure 5A, serum TG levels were ~30%—35% lower in both male and female IKO mice compared to controls. Similarly, serum NEFA and free cholesterol levels were significantly decreased or trending towards decrease in IKO mice, whereas total cholesterol levels were not changed in IKO mice (Figure 5B—D). Plasma lipoprotein profiling analysis revealed a marked decrease in TG levels in chylomicron/VLDL fraction in IKO mice upon fasting/HFD refeeding (Figure 5E), while cholesterol levels were decreased in all lipoprotein fractions in IKO serum (Figure 5F). Similar to oil gavage, HFD refeeding resulted in massive lipid accumulation in both duodenum and jejunum of IKO mice as revealed by histology analysis and Oil red O staining (Figure 5G,H), indicating defective TG output in the absence of SEC16B.

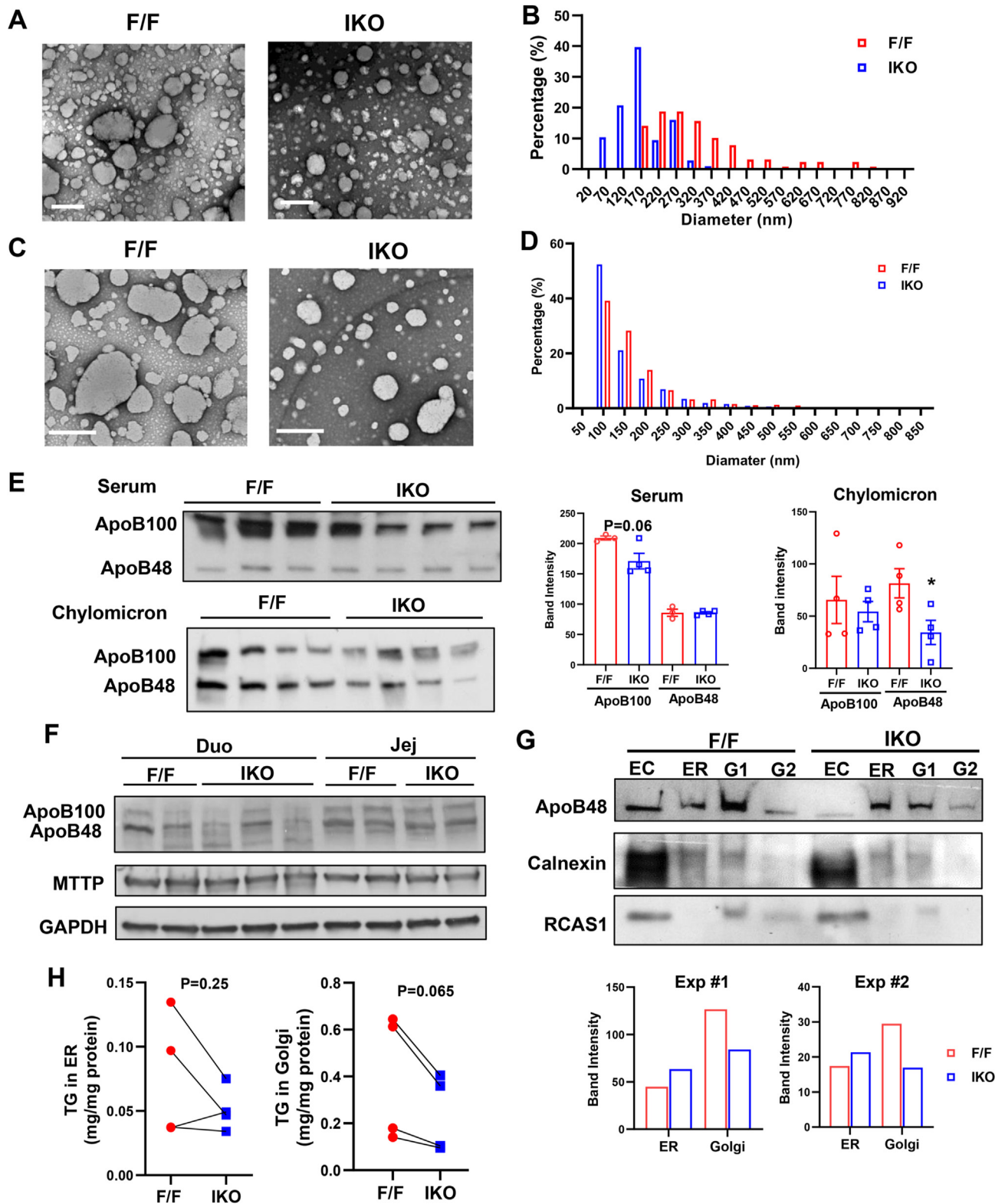### 3.4. Loss of *Sec16b* impairs chylomicron lipidation and secretion

To understand how loss of *Sec16b* affects lipid absorption, we first examined the expression of genes involved in lipid metabolism in the intestines of overnight fasting and HFD refeeding mice. The mRNA levels of acyl-CoA synthase long chain family member 5 (*Acsl5*) and monoacylglycerol O-acyltransferase 2 (*Mogat2*), two genes in the TG synthesis pathway in enterocytes, were significantly decreased in male IKO jejunum compared to controls after overnight fasting (Fig. S9A). There was also a trend of decrease in the expression of *Mttp* (P = 0.06) in male IKO intestines. However, the changes in their expression were abolished upon HFD refeeding (Fig. S9B). Furthermore, there was no significant change in the expression of these genes in female IKO mice compared to controls in either fasting or refeeding

conditions (Figs. S9C and S9D). We further examined their expression in *in vitro* 2D organoid cultured cells treated with oleic acid. As shown in Fig. S10A, *Apob*, *Dgat2*, *Mttp* and *Fatp1* mRNA levels were decreased, while *Mogat2* and *Fabp2* mRNA levels were increased in IKO cells. Nevertheless, these data indicate that altered expression of lipid metabolic genes alone is unlikely to cause impaired lipid absorption in IKO mice.

Dietary lipids are absorbed into circulation in the form of chylomicron. We next investigated if intestinal *Sec16b* deficiency affects chylomicron assembly and secretion upon HFD refeeding. Negative staining of plasma chylomicron fractions by electron microscopy revealed markedly smaller chylomicron particles in *Sec16b* IKO mice compared to controls (Figure 6A,B). The size of chylomicrons is modulated by the lipidation of apoB48 and TG lipolysis in circulation. To determine if lipolysis contributes to smaller chylomicrons in IKO mice, we pretreated mice with lipase inhibitor and measured chylomicron size after HFD refeeding. As shown in Figure 6C,D, chylomicrons of IKO mice were smaller than those of control mice in the presence of lipase inhibitor, albeit to a less extent compared to nontreated mice. Together with the observation that no difference in LPL activity was observed in HFD refed control and IKO mice (Fig. S7E), these data suggested that lipolysis is unlikely to be a major cause of reduced chylomicron size in IKO mice. Western blot analysis showed that apoB48 levels in the chylomicron fraction were decreased in *Sec16b* IKO mice, while total serum apoB48 levels were comparable (Figure 6E), indicating that chylomicron secretion is impaired in the setting of SEC16B deficiency. Interestingly, we did not observe accumulation of apoB48 in the intestine of IKO mice or *in vitro* cultured cells treated with oleic acid (Figure 6F, Figure S10B), likely because its degradation was enhanced due to poor lipidation. Despite reduced apoB lipidation, MTTP protein levels were comparable in IKO and control mice after 2 h of HFD refeeding (Figure 6F). Interestingly, MTTP protein levels were increased in oleic acid treated IKO cells compared to control cells (Fig. S10B). Nonetheless, these data indicate that impaired lipidation in IKO mice is unlikely caused by altered MTTP. To further investigate if SEC16B affects PCTV trafficking within enterocytes, we isolated ER and Golgi fractions from enterocytes of HFD refed mice, and analyzed the distribution of apoB in ER and Golgi. As shown in Figure 6G, apoB48 level was slightly higher in ER fraction, but much lower in Golgi fraction of IKO enterocytes compared to controls. Furthermore, TG content was lower in the Golgi fractions from IKO mice compared to those from control mice (Figure 6H), indicating that loss of *Sec16b* likely blunts the transport of PCTV from ER to Golgi. However, we did not observe significant accumulation of TG in the ER fractions of IKO mice (Figure 6H). Instead, TG levels in the ERs of IKO trended towards a decrease compared to controls, suggesting that *Sec16b* deficiency may affect the transfer of TG into ER lumen for chylomicron packaging.

To obtain further insight into the mechanism of the chylomicron production defect in *Sec16b* IKO mice, we examined intestine samples by electron microscopy (EM). Consistent with more lipid accumulation in HFD refed IKO intestines, EM analysis showed much bigger cytosolic lipid droplets (CLDs) in IKO enterocytes (Figure 7A). Lipoprotein particles were easily visualized in the secretory vesicles and Golgi apparatus of control enterocytes (Figure 7B,C). In contrast, lipoprotein particles were markedly smaller and less stained in the secretory vesicles of IKO enterocytes, further corroborating poor apoB48 lipidation in the absence of SEC16B. We did not observe noticeable lipoprotein particles in the Golgi apparatus of IKO enterocytes (Figure 7C). Consistent with reduced TG levels in ER fractions, lipid droplets in the ERs were also smaller in IKO enterocytes compared to controls. Consistent with impaired lipid absorption, lipoprotein particles
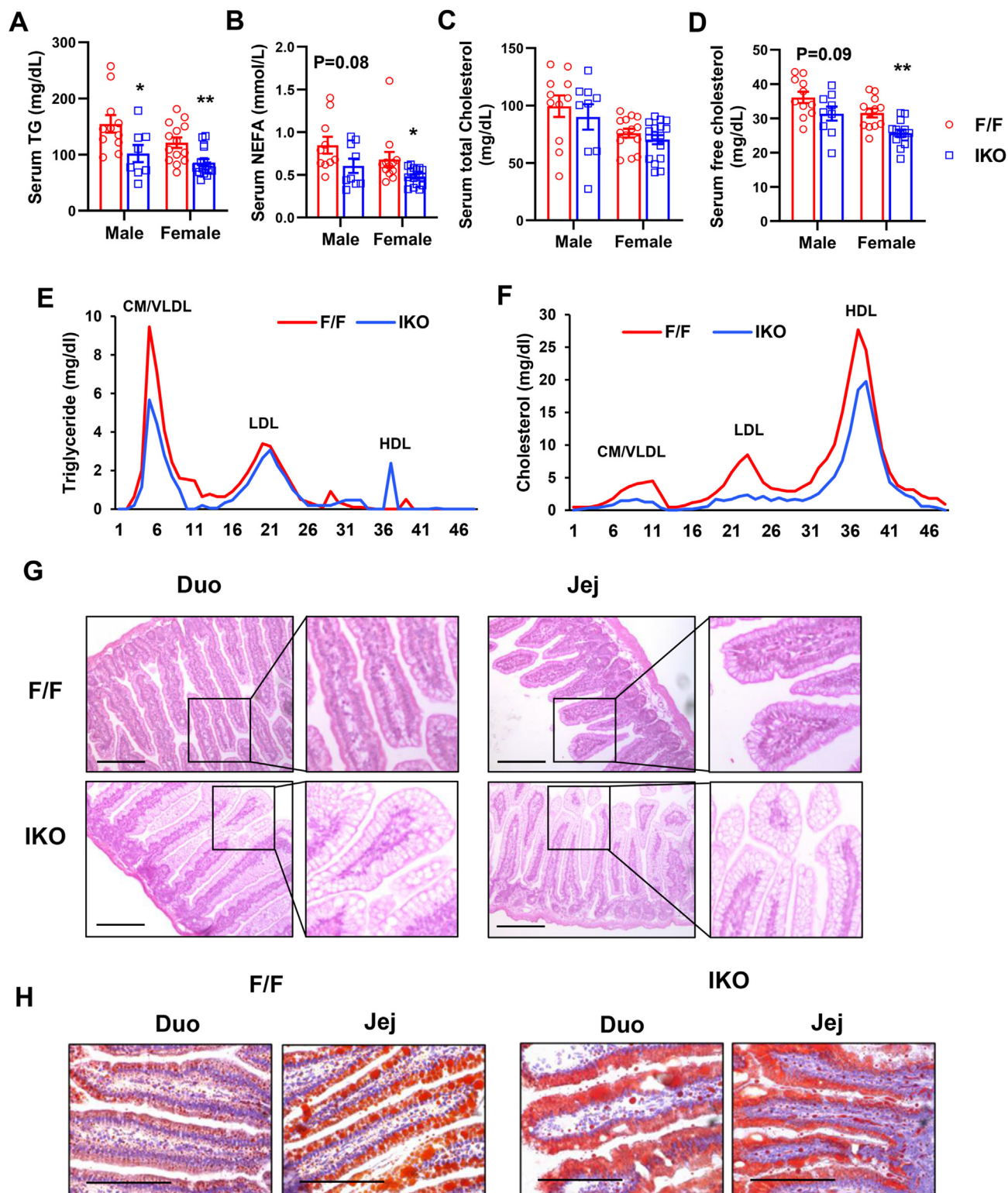
Figure 5: Loss of *Sec16b* in the intestine impairs lipid absorption during fasting and HFD refeeding. (A−D) Plasma lipid levels in chow diet fed control (F/F) and IKO mice after fasting overnight and refeeding HFD for 2 h (n = 9−16/group). **(E−F)** Plasma from control (F/F) and IKO mice fasted overnight and refed with HFD for 2 h was pooled (*n* = 5). Lipoprotein profiles were analyzed by fast protein liquid chromatography (FPLC). **(G)** Representative histology of intestine sections from control (F/F) and IKO mice as in A-D. Scale bar: 100 μm. **(H)** Representative oil-red-O staining of intestine sections from control (F/F) and IKO mice as in A-D. Scale bar: 100 μm. Values are means ± SEM. Statistical analysis was performed with Student's t test (A-D). *P < 0.05, **P < 0.01, ***P < 0.001.

Figure 6: *Sec16b* deficiency in the intestine impairs chylomicron lipidation and secretion. (A) Representative images of negative staining of chylomicrons. Chow diet fed mice were fasted overnight and refed 60% HFD for 2 h. Chylomicrons were isolated and pooled from 5 mice/group. Chylomicrons were stained with 2.0% uranyl acetate and visualized by electron microscopy. Scale bar: 500 nm. **(B)** Quantification of chylomicron particle size in (A). **(C–D)** Negative staining and quantification of plasma chylomicron particle size in lipase inhibitor treated control (F/F) and IKO mice. Chow diet fed mice were fasted overnight and retro-orbitally injected with Tyloxapol followed by 60% HFD refeeding for 2h. Scale bar: 500 nm. **(E)** ApoB western blot in whole serum and chylomicron fraction of control (F/F) and IKO mice as in (A). **(F)** ApoB western blot in duodenum and jejunum of control (F/F) and IKO mice as in (A). **(G)** ApoB western blot in endoplasmic reticulum (ER) and Golgi isolated from the enterocytes of control (F/F) and IKO mice as in (A). EC: enterocyte whole cell lysate, G1: Golgi fraction #1, G2: Golgi fraction #2. Quantification of two experiments were shown. **(H)** Triglyceride content in ER and Golgi fractions isolated from the enterocytes of control (F/F) and IKO mice as in (A). Each pair represents one experiment from enterocytes of two control and two IKO mice. Statistical analysis was performed with paired Student's t test.
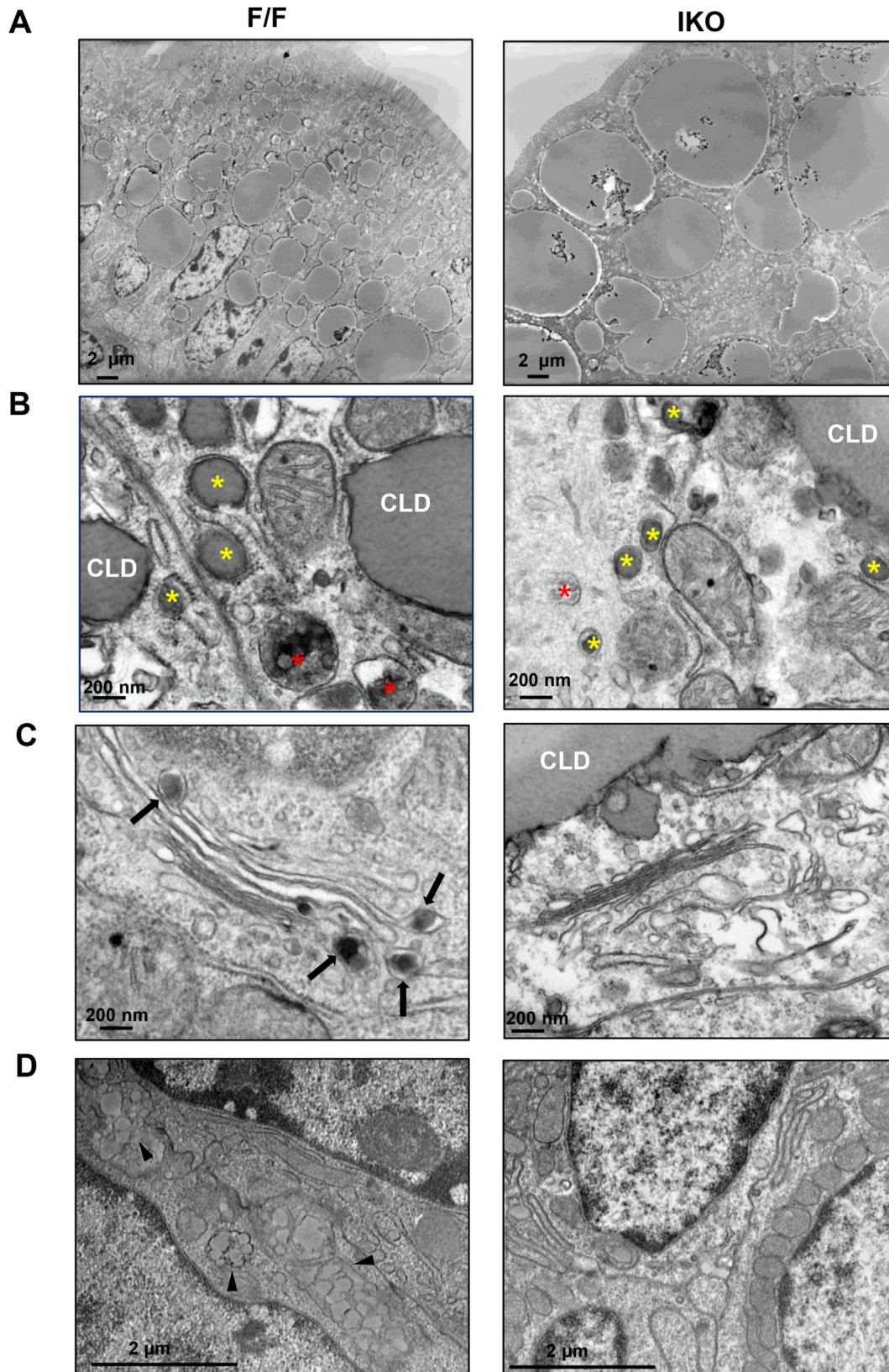
Figure 7: Reduced chylomicron secretion in *Sec16b* deficient enterocytes. (A–D) Electron microscopy analysis of intestine sections from control (F/F) and IKO. Chow diet fed mice were fasted overnight and refed 60% HFD for 2 h. Red stars denote secretory vesicles containing lipoprotein particles. Yellow stars indicate TG in the lumen of ER. Arrows indicate TG in the Golgi apparatus. Arrowheads indicate chylomicrons in the intercellular space. CLD: cytosolic lipid droplet.

were almost undetectable in the intercellular space of IKO intestines (Figure 7D). These data suggest that SEC16B regulates enterocyte TG distribution and chylomicron transport in enterocytes.

4. DISCUSSION

The small intestine plays an important role in modulating lipid homeostasis by controlling lipid absorption. Excess lipid absorption is one of the major risk factors of obesity and metabolic disorders [2,32]. The absorption of dietary lipids involves several steps, including the uptake of FA and monoacylglycerol from intestinal lumen, resynthesis of TG, chylomicron assembly, lipidation and secretion [3,4,8]. Although the molecular mechanisms modulating these steps have been extensively investigated, the regulation of chylomicron transport and secretion in enterocytes remains poorly understood. Here we have shown that loss of *Sec16b* in intestine impairs lipid absorption likely through blocking chylomicron transport from ER to Golgi and impeding the lipidation of prechylomicrons. These findings implicate that SEC16B is a critical regulator of chylomicron maturation and secretion.

Previous studies have shown that SEC16 is localized at transitional ER (tER), where they function as scaffold proteins to direct the organization of ERES in yeast and *Drosophila* [25,33,34]. SEC16 interacts with SEC23, SEC24 and SEC31 in COPII machinery and control its exit from ER to Golgi in the secretory pathway [35,36]. It is well documented that COPII proteins are involved in the transport of proteins and lipoprotein particles, including chylomicrons [3,37,38]. Therefore, SEC16 has been proposed to regulate protein and lipid transport. Several studies demonstrated that mutations in *Sec16* gene result in the accumulation of secretory proteins and lack of secretory vesicles in the cell [25,39–41], corroborating that SEC16 participates in protein secretion. However, whether SEC16 modulates lipid secretion has not been investigated. Mammalian cells contain two *Sec16* homologs, SEC16A and SEC16B, which both localize at ERES [41]. SEC16A is the primary homolog of yeast Sec16 as they have similar molecular mass [42]. SEC16A interacts with SEC23 and SEC13 of COPII vesicles and facilitate COPII vesicle budding from the ER, thereby regulating protein secretion [42,43]. Compared to SEC16A, SEC16B protein lacks Sec23-interacting C-terminal domain [41]. SEC16B plays a minor role in protein secretion as depletion of SEC16B has a lesser effect compared to loss of SEC16A [28]. Moreover, overexpression of SEC16B cannot compensate the defect in protein secretion caused by SEC16A knockdown [44]. Furthermore, we showed that loss of SEC16B in intestine does not result in discernible phenotype on chow diet despite the fact that small intestine is an important endocrine organ that secrets gut hormones, indicating that SEC16B is unlikely to play critical roles in protein secretion.

Interestingly, SEC16A and SEC16B show different tissue distribution in mammals. SEC16A is ubiquitously expression in most tissues, while SEC16B is highly expressed in the liver and intestine (data not shown), suggesting that they may have distinct functions in these organs. Considering that the liver and small intestine are the major organs for lipoprotein production in the body, we hypothesized that SEC16B may be involved in lipoprotein metabolism. Our data showed that *Sec16b* deficiency in intestine impairs lipid absorption, supporting a critical role in chylomicron metabolism. In addition, we did not observe compensatory effect in defective lipid absorption by endogenous SEC16A in IKO mice, suggesting that the function in regulating lipid metabolism is likely unique to SEC16B. But how SEC16B acquires this specialized function during evolution is still unclear. Compared to SEC16A, SEC16B lacks a C-terminal conserved domain that interacts with other proteins [41]. Thus, it is possible that SEC16B interacts with a different set of proteins in metabolic tissues *in vivo* to fulfill its function in lipid metabolism.

Our mechanistic studies revealed that loss of *Sec16b* blunts lipid absorption mainly through blocking its transport from the ER to Golgi and inhibiting chylomicron lipidation. Given that SEC16B localizes to ERES and interacts with COPII components, it is reasonable to speculate that it may regulate COPII exit from ER, and thereby modulating chylomicron trafficking. But the observation that IKO mice have reduced chylomicron lipidation is surprising since there was no difference in MTTP protein levels in control and IKO intestines. Our data showed that IKO enterocytes contained much bigger cytosolic lipid droplets and less TG in the ERs compared to controls. Considering that the biogenesis of both lipid droplets and chylomicrons are initiated in the ER, we speculate that lipids may be channeled to lipid droplets instead of being transferred into the ER for chylomicron assembly in IKO mice. Further studies will be needed to determine if SEC16B is involved in the partitioning of lipids into cytosolic lipid droplets and chylomicrons.

Numerous GWAS studies have demonstrated that several SNPs in *SEC16B* gene locus are associated with obesity and BMI. For examples, the minor "C" variant of rs10913469 in the intron of *SEC16B* is more common in adults and children with obesity and higher BMI in Asia, Mexico, and several European countries [17,19,45,46]. Similarly, the intergenic "G" variant of rs543874 is associated with higher obesity rate and body fat percentage in Africa American, East Asian and European descent [21—23]. However, it is unclear how these variants may affect body weight and fat mass in the body. It would be interesting to examine if these variants affect the expression of SEC16B and whether overexpression of SEC16B increases lipid absorption and adiposity. Interestingly, genetic variants in *SEC16B* have been shown to be associated with obesity more significantly in women [15,47], which is consistent with our observation that the difference in body weight gain on HFD was more dramatic in female IKO mice than males. The mechanisms underlying gender difference in the roles of SEC16B in obesity merits further investigation.

In summary, these results revealed a novel regulator of the biogenesis and transport of chylomicron, and thereby controlling lipid absorption and obesity. Future studies will explore whether targeting SEC16B could be used as a strategy to modulate diet-induced obesity.

AUTHOR CONTRIBUTIONS

R.S. designed and performed experiments, analyzed data, and wrote the paper. W.L. and Y.T. performed experiments and analyzed data. B.W. conceived the project, designed experiments, analyzed data, supervised the project, and wrote the paper.

DATA AVAILABILITY

Data will be made available on request.

ACKNOWLEDGEMENTS

CONFLICT OF INTEREST

None declared.

APPENDIX A. SUPPLEMENTARY DATA

Supplementary data to this article can be found online at https://doi.org/10.1016/j.molmet.2023.101693.

REFERENCES

[1] Malik VS, Willett WC, Hu FB. Global obesity: trends, risk factors and policy implications. Nat Rev Endocrinol 2013;9(1):13—27.

[2] Bluher M. Obesity: global epidemiology and pathogenesis. Nat Rev Endocrinol 2019;15(5):288—98.

[3] Mansbach CM, Siddiqi SA. The biogenesis of chylomicrons. Annu Rev Physiol 2010;72:315—33.

[4] Abumrad NA, Davidson NO. Role of the gut in lipid homeostasis. Physiol Rev 2012;92(3):1061—85.

[5] Ko CW, Qu J, Black DD, Tso P. Regulation of intestinal lipid metabolism: current concepts and relevance to disease. Nat Rev Gastroenterol Hepatol 2020;17(3):169—83.

[6] Hussain MM, Shi J, Dreizen P. Microsomal triglyceride transfer protein and its role in apoB-lipoprotein assembly. J Lipid Res 2003;44(1):22—32.

[7] Siddiqi SA, Gorelick FS, Mahan JT, Mansbach 2nd CM. COPII proteins are required for Golgi fusion but not for endoplasmic reticulum budding of the pre-chylomicron transport vesicle. J Cell Sci 2003;116(Pt 2):415—27.

[8] Dash S, Xiao C, Morgantini C, Lewis GF. New insights into the regulation of chylomicron production. Annu Rev Nutr 2015;35:265—94.

[9] Mansbach 2nd CM, Nevin P. Intracellular movement of triacylglycerols in the intestine. J Lipid Res 1998;39(5):963—8.

[10] Mansbach CM, Dowell R. Effect of increasing lipid loads on the ability of the endoplasmic reticulum to transport lipid to the Golgi. J Lipid Res 2000;41(4):605—12.

[11] Nauli AM, Nassir F, Zheng S, Yang Q, Lo CM, Vonlehmden SB, et al. CD36 is important for chylomicron formation and secretion and may mediate cholesterol uptake in the proximal intestine. Gastroenterology 2006;131(4):1197—207.

[12] Drover VA, Ajmal M, Nassir F, Davidson NO, Nauli AM, Sahoo D, et al. CD36 deficiency impairs intestinal lipid secretion and clearance of chylomicrons from the blood. J Clin Invest 2005;115(5):1290—7.

[13] Neeli I, Siddiqi SA, Siddiqi S, Mahan J, Lagakos WS, Binas B, et al. Liver fatty acid-binding protein initiates budding of pre-chylomicron transport vesicles from intestinal endoplasmic reticulum. J Biol Chem 2007;282(25):17974—84.

[14] Siddiqi S, Saleem U, Abumrad NA, Davidson NO, Storch J, Siddiqi SA, et al. A novel multiprotein complex is required to generate the prechylomicron transport vesicle from intestinal ER. J Lipid Res 2010;51(7):1918—28.

[15] Xi B, Shen Y, Reilly KH, Zhao X, Cheng H, Hou D, et al. Sex-dependent associations of genetic variants identified by GWAS with indices of adiposity and obesity risk in a Chinese children population. Clin Endocrinol 2013;79(4):523—8.

[16] Albuquerque D, Nobrega C, Rodriguez-Lopez R, Manco L. Association study of common polymorphisms in MSRA, TFAP2B, MC4R, NRXN3, PPARGC1A, TMEM18, SEC16B, HOXB5 and OLFM4 genes with obesity-related traits among Portuguese children. J Hum Genet 2014;59(6):307—13.

[17] Hotta K, Nakamura M, Nakamura T, Matsuo T, Nakata Y, Kamohara S, et al. Association between obesity and polymorphisms in SEC16B, TMEM18, GNPDA2, BDNF, FAIM2 and MC4R in a Japanese population. J Hum Genet 2009;54(12):727—31.

[18] Sahibdeen V, Crowther NJ, Soodyall H, Hendry LM, Munthali RJ, Hazelhurst S, et al. Genetic variants in SEC16B are associated with body composition in black South Africans. Nutr Diabetes 2018;8(1):43.

[19] Thorleifsson G, Walters GB, Gudbjartsson DF, Steinthorsdottir V, Sulem P, Helgadottir A, et al. Genome-wide association yields new sequence variants at seven loci that associate with measures of obesity. Nat Genet 2009;41(1):18—24.

[20] Zeggini E, Scott LJ, Saxena R, Voight BF, Marchini JL, Hu T, et al. Meta-analysis of genome-wide association data and large-scale replication identifies additional susceptibility loci for type 2 diabetes. Nat Genet 2008;40(5):638—45.

[21] Monda KL, Chen GK, Taylor KC, Palmer C, Edwards TL, Lange LA, et al. A meta-analysis identifies new loci associated with body mass index in individuals of African ancestry. Nat Genet 2013;45(6):690—6.

[22] Lu Y, Day FR, Gustafsson S, Buchkovich ML, Na J, Bataille V, et al. New loci for body fat percentage reveal link between adiposity and cardiometabolic disease risk. Nat Commun 2016;7:10495.

[23] Vogelezang S, Bradfield JP, Ahluwalia TS, Curtin JA, Lakka TA, Grarup N, et al. Novel loci for childhood body mass index and shared heritability with adult cardiometabolic traits. PLoS Genet 2020;16(10):e1008718.

[24] Novick P, Field C, Schekman R. Identification of 23 complementation groups required for post-translational events in the yeast secretory pathway. Cell 1980;21(1):205—15.

[25] Espenshade P, Gimeno RE, Holzmacher E, Teung P, Kaiser CA. Yeast SEC16 gene encodes a multidomain vesicle coat protein that interacts with Sec23p. J Cell Biol 1995;131(2):311—24.

[26] Yamaguchi M. Novel protein RGPR-p117: its role as the regucalcin gene transcription factor. Mol Cell Biochem 2009;327(1—2):53—63.

[27] Yamaguchi M, Misawa H, Ma ZJ. Novel protein RGPR-p117: the gene expression in physiologic state and the binding activity to regucalcin gene promoter region in rat liver. J Cell Biochem 2003;88(6):1092—100.

[28] Tani K, Tagaya M, Yonekawa S, Baba T. Dual function of Sec16B: endoplasmic reticulum-derived protein secretion and peroxisome biogenesis in mammalian cells. Cell Logist 2011;1(4):164—7.

[29] Yonekawa S, Furuno A, Baba T, Fujiki Y, Ogasawara Y, Yamamoto A, et al. Sec16B is involved in the endoplasmic reticulum export of the peroxisomal membrane biogenesis factor peroxin 16 (Pex16) in mammalian cells. Proc Natl Acad Sci U S A 2011;108(31):12746—51.

[30] Folch J, Lees M, Sloane Stanley GH. A simple method for the isolation and purification of total lipides from animal tissues. J Biol Chem 1957;226(1):497—509.

[31] Wang B, Rong X, Duerr MA, Hermanson DJ, Hedde PN, Wong JS, et al. Intestinal phospholipid remodeling is required for dietary-lipid uptake and survival on a high-fat diet. Cell Metabol 2016;23(3):492—504.

[32] Klop B, Elte JW, Cabezas MC. Dyslipidemia in obesity: mechanisms and potential targets. Nutrients 2013;5(4):1218—40.

[33] Connerly PL, Esaki M, Montegna EA, Strongin DE, Levi S, Soderholm J, et al. Sec16 is a determinant of transitional ER organization. Curr Biol 2005;15(16):1439—47.

[34] Ivan V, de Voer G, Xanthakis D, Spoorendonk KM, Kondylis V, Rabouille C. Drosophila Sec16 mediates the biogenesis of tER sites upstream of Sar1 through an arginine-rich motif. Mol Biol Cell 2008;19(10):4352—65.

[35] Gimeno RE, Espenshade P, Kaiser CA. COPII coat subunit interactions: Sec24p and Sec23p bind to adjacent regions of Sec16p. Mol Biol Cell 1996;7(11):1815—23.

[36] Shaywitz DA, Espenshade PJ, Gimeno RE, Kaiser CA. COPII subunit interactions in the assembly of the vesicle coat. J Biol Chem 1997;272(41):25413—6.

[37] Zanetti G, Pahuja KB, Studer S, Shim S, Schekman R. COPII and the regulation of protein sorting in mammals. Nat Cell Biol 2011;14(1):20—8.

[38] Jones B, Jones EL, Bonney SA, Patel HN, Mensenkamp AR, Eichenbaum-Voline S, et al. Mutations in a Sar1 GTPase of COPII vesicles are associated with lipid absorption disorders. Nat Genet 2003;34(1):29–31.

[39] Kaiser CA, Schekman R. Distinct sets of SEC genes govern transport vesicle formation and fusion early in the secretory pathway. Cell 1990;61(4): 723–33.

[40] Watson P, Townley AK, Koka P, Palmer KJ, Stephens DJ. Sec16 defines endoplasmic reticulum exit sites and is required for secretory cargo export in mammalian cells. Traffic 2006;7(12):1678–87.

[41] Bhattacharyya D, Glick BS. Two mammalian Sec16 homologues have nonredundant functions in endoplasmic reticulum (ER) export and transitional ER organization. Mol Biol Cell 2007;18(3):839–49.

[42] Iinuma T, Shiga A, Nakamoto K, O'Brien MB, Aridor M, Arimitsu N, et al. Mammalian Sec16/p250 plays a role in membrane traffic from the endoplasmic reticulum. J Biol Chem 2007;282(24):17632–9.

[43] Hughes H, Budnik A, Schmidt K, Palmer KJ, Mantell J, Noakes C, et al. Organisation of human ER-exit sites: requirements for the localisation of Sec16 to transitional ER. J Cell Sci 2009;122(Pt 16):2924–34.

[44] Budnik A, Heesom KJ, Stephens DJ. Characterization of human Sec16B: indications of specialized, non-redundant functions. Sci Rep 2011;1:77.

[45] Zhao X, Xi B, Shen Y, Wu L, Hou D, Cheng H, et al. An obesity genetic risk score is associated with metabolic syndrome in Chinese children. Gene 2014;535(2):299–302.

[46] Jimenez-Osorio AS, Aguilar-Lucio AO, Cardenas-Hernandez H, Musalem-Younes C, Solares-Tlapechco J, Costa-Urrutia P, et al. Polymorphisms in adipokines in Mexican children with obesity. Internet J Endocrinol 2019;2019: 4764751.

[47] Shi J, Long J, Gao YT, Lu W, Cai Q, Wen W, et al. Evaluation of genetic susceptibility loci for obesity in Chinese women. Am J Epidemiol 2010;172(3): 244–54.